

Waveguide Tailored Radiation Pattern of Nanoparticles for Tunable Multimodal Guided Surface Lattice Resonances in Asymmetric Environment

Suichu Huang¹, Kan Yao², Wentao Huang¹, Xuezheng Zhao^{1,*}, Yuebing Zheng^{2,*}, Yunlu Pan^{1,*}

¹ Key Laboratory of Micro-Systems and Micro-Structures Manufacturing of Ministry of Education and School of Mechatronics Engineering, Harbin Institute of Technology, Harbin 150001, China

² Walker Department of Mechanical Engineering, Material Science and Engineering Program and Texas Material Institute, The University of Texas at Austin, Austin TX 78712, United States

*Corresponding author. Email: zhaoxz@hit.edu.cn, zheng@austin.utexas.edu, yunlupan@hit.edu.cn

Abstract

Surface lattice resonances (SLR) in metasurfaces is promising in applications of sub-wavelength devices, with high quality factors (high-Q), large local field enhancement and long-range interaction properties. Tunable peak position and multimodal resonances make SLR further appealing to flexible and multiple light-matter interactions. However, reported multimodal SLRs lack flexible and economic tunability. Moreover, current high-Q SLR requires a homogeneous index of operational environment, which hampered potential applications such as biosensors that are usually operated in aqueous or air environment. Here we report a guided-SLR (gSLR) that is easily accessible in index-discontinuous environment along with multimodal property and active tunability of resonating wavelength, mode number and mode coupling strength. The gSLR is realized via coupling scattered light from metasurfaces' units into a slab waveguide, which opens up a light propagating channel in the lattice plane in index-asymmetric environment. Tailoring radiation pattern of each units with guided transverse electric (TE) and transverse magnetic (TM) modes, multimodal resonances of both orthogonal and parallel coupling directions are accomplished. Mode number and mode frequency positions can be easily adjusted by waveguide configuration, while mode strength is tuned by vertical position in the slab. The easy-to-access, actively tunable and multimodal gSLR in inhomogeneous medium will promote the realization of ultrathin and ultracompact nano-optical and optoelectronic devices.

Key Words: Surface Lattice Resonances, Waveguide, Multimode, Radiation Pattern, Plasmonics

1 Introduction

With the ability to confine light in sub-wavelength range and to largely enhance local field, sub-wavelength plasmonic nanostructures are of great interests in many field, such as nanolasing^{1,2}, optic switching^{3,4}, biosensing^{5,6}, non-linear optical process^{7,8}, metasurfaces^{9,10} and bound states in the continuum^{11,12}. Individual sub-wavelength plasmonic nanostructures support localized surface plasmon resonances (LSPR), where the free-electron plasma at the metal-dielectric interface couples to the oscillating electromagnetic waves¹³. The local field enhancement allows plasmonic nanoparticles to play rich roles in applications like light-matter interaction studies^{14,15} and sensing^{16,17}. However, potential applications of plasmonic nanoparticles or clusters are hindered by their low quality-factors (Q-factor), due to intrinsic losses of plasmonic materials at optical frequencies¹⁸⁻²⁰.

A practical way to largely increase Q-factor of plasmonic nanostructures is arranging nanoparticles into organized lattices. When the radiative LSPR modes of individual nanoparticle match in-plane diffraction modes of the lattice, a so-called surface lattice resonance (SLR) emerges, where the loss of individual units is supplemented by the scattered field from adjacent ones, resulting in high Q-factors^{18,21-23}. Through carefully designing, plasmonic metasurface with a Q-factor over 2000 has been reported²⁰. According to the type of LSPR mode that couples to diffraction modes, SLR can be classified into dipole lattice resonances, quadrupole lattice resonances and superlattice resonances²⁴, among which the dipole lattice resonance draws more interests since resonating dipoles in a metasurface can easily be accessed by a beam propagating in free space and require only a sub-wavelength propagation region for operation²⁰.

A vital prerequisite for excitation of high Q-factor (high-Q) in-plane SLR is careful index-matching of superstrate and substrate^{21,25,26}. An index discontinuous substrate tends to destruct the in-plane coupling of an array²⁵, but is necessary for many fabrication techniques and application scenarios. Immersing the substrate-supported array into an index matching

liquid can be an expedience^{27,28}, but is not a versatile solution for different kinds of applications, for example, biosensing, where the superstrate is usually air or water^{29,30}. Recently, a few SLR in index mismatched environment have been reported³¹⁻³⁵, where the implementation is achieved by engineering the particle geometry^{31,32} or introducing a metal substrate³³⁻³⁵. However, their obtained Q-factors are low and explanations of these SLRs in asymmetric environment are slightly ambiguous. A theoretically unequivocal and widely adaptable method to realize high-Q resonances in asymmetrical environment is in need.

Though most SLR studies focus on single mode resonance, some applications, requiring enhancement of light-matter interactions at different wavelength simultaneously, for example, multimodal lasing^{36,37}, leads to the exploration of multimodal SLR³⁸⁻⁴². Implementations based on lattice hybridization^{38,39}, band structure engineering^{37,40} and multi-reflection at a close boundary^{41,42} have been achieved. However, these methods require elaborate lattice design, have limited SLR mode number and lack active tunability. In the meantime, controlling of mode coupling strength is merely reported. An economic way to realize abundant resonant modes with flexible tunability is still demanded.

Coupling direction is another widely discussed topic in SLR studies. Controlling the coupling direction of SLR can facilitate the application in many fields, for example, optical communication⁴³. Under the discrete-dipole modeling, the oscillation direction or dipole moment of individual resonator determines the coupling direction of SLR⁴⁴. Most reported plasmonic SLRs are orthogonally coupled because metallic nanoparticles show radiative behavior close to electric dipoles (ED)⁴⁵. Parallel coupling is usually observed in dielectric metasurface due to magnetic dipole (MD) modes in large dielectric nanoparticles^{46,47}. Though, a few parallelly coupled plasmonic SLR phenomena have been observed^{35,48-50}, a rational way to control the coupling direction are still concealed.

Inspired by these demands, here we propose and experimentally demonstrate a tunable multimodal guided-SLR (gSLR) that adapts highly contrast index environment, through embedding the metasurface in a slab waveguide. The slab waveguide is introduced to modulate radiation patterns of individual nanoparticles in the array and works in two folds. On one hand, the slab waveguide opens up an in-plane propagating channel for scattered light from nanoparticles in highly contrasted environment, giving access to SLR. On the other, the

rich perpendicularly transmitting transverse electric (TE) and transverse magnetic (TM) modes endow gSLR with multiple resonant modes in orthogonal coupling directions. Resonant peak number and wavelength of each peak of a fixed array configuration can be conveniently adjusted by controlling slab thickness and cladding index. Coupling directions at interested wavelength is adjustable according to guided modes. Moreover, coupling strength of a specific gSLR mode is able to be tuned by vertical position of the array in the slab. The tunable multimodal gSLR presented here will enrich the colorful SLR world and lead paths to novel nano-plasmonic devices.

2 Results and Discussion

2.1 Slab waveguide tailored radiation pattern for multimodal gSLR

The gold nanoparticle array (AuNPA) metasurface in consideration is fabricated on a quartz substrate ($n \approx 1.45$) by a template-based method and annealed to improve uniformity⁵¹, with lattice constants of 600 nm in x-direction (p_x) and 550 nm in y-direction (p_y) (**Fig. 1a**). Rectangular unit cell is chosen here that different resonant modes can be distinguished by peak positions in the spectrum. To enable gSLR, a dielectric slab with index higher than the substrate and superstrate is deposited to form a slab waveguide, with the AuNPA metasurface embedded in the slab (insert in **Fig. 1a**). Being buried in a slab waveguide, a portion of scattered light from individual nanoparticles will couple into the waveguide. Similar to guided mode resonances (GMR)^{52,53}, once the scattered light couples to a guided mode whose wave vector is an integer multiple of the metasurface lattice constants, nanoparticles in this light transmitting direction will be re-excited by this guided light and oscillate in phase, thus a collective resonance is triggered. Unlike GMR where light is coupled into the waveguide by diffractions of gratings or meta-gratings and won't interact with the grating any more, guided light in the discussed resonances is injected by scattering of consisting nanoparticles and re-excite other nanoparticles in the coupling direction, which is same as the situation in classic SLR. Based on these characteristics, we define it as guided surface lattice resonance (gSLR). The gSLR mode dispersion relationship can be derived from slab waveguide theory as

$$\tan(\beta_2 t_{\text{slab}}) = \frac{\beta_2(c_{21}\beta_1 + c_{23}\beta_3)}{\beta_2^2 - c_{21}\beta_1 c_{23}\beta_3} \quad (1)$$

where t_{slab} is thickness of the slab, $\beta_1 = \sqrt{k^2 - n_1^2 k_0^2}$, $\beta_2 = \sqrt{n_2^2 k_0^2 - k^2}$, $\beta_3 =$

$\sqrt{k^2 - n_1^2 k_0^2}$, $k = \sqrt{(2\pi m/p_x)^2 + (2\pi n/p_y)^2}$ is the wave vector in the coupling direction, $k_0 = \frac{2\pi}{\lambda}$ is wave vector in vacuum and λ is wavelength, c_{21} and c_{23} are coefficients, for TE modes, $c_{21} = c_{23} = 1$, for TM modes, $c_{21} = n_{\text{slab}}^2/n_{\text{sup}}^2$ and $c_{23} = n_{\text{slab}}^2/n_{\text{sub}}^2$. The cut-off thickness, the thinnest thickness of the slab to support a guided mode of a given wavelength, can be derived as

$$t_c = \frac{\lambda}{2\pi\sqrt{n_{\text{slab}}^2 - n_{\text{sub}}^2}} \left[\arctan \left(c_{21} \sqrt{\frac{n_{\text{sub}}^2 - n_{\text{sup}}^2}{n_{\text{slab}}^2 - n_{\text{sub}}^2}} \right) + j\pi \right], j = 0, 1, 2, \dots \quad (2)$$

In an air-photoresist-quartz configuration ($n_{\text{sup}}=1$, $n_{\text{slab}}=1.56$, $n_{\text{sub}}=1.45$), multiple resonant peaks show up once the slab thickness surpasses the cut-off thickness and red shift as the increase of slab thickness (**Fig. 1b** and **Fig. S1**). The simulated gSLR modes evolution matches the dispersion relationship very well. To experimentally observe gSLR mode evolution, a slab with gradually increasing thickness is deposited by a layer-by-layer spincoating and curing of photoresist (SU8, see Method for more experiment details). The measured results closely match simulations (**Fig. 1c, a** and **f**). The peak split in experiment results is originated from a small portion of obliquely incident light⁵⁴. When there is no slab layer, the collective resonance in such a highly contrasted medium ($n_{\text{sup}}/n_{\text{sub}} = 1/1.45$) is inhibited (**Fig. 1d**), because of the destructive influence of substrate²⁵. When looking into the radiation pattern of an AuNP on substrate, it can be found that the radiation pattern is tailored into three lobes, with one into superstrate and two into substrate, leaving no section at horizontal plane (**Fig. 1e**). When the slab thickness is larger than guided modes cut-off thicknesses, narrow TE and TM gSLR peaks appear (**Fig. 1f**). By fitting these two peaks with the Fano formula, the Q-factors are calculated to be 183 and 440, respectively (**Fig. S6**), which is comparable to reported high-Q studies^{27,37,55,56}. The TM₀(±1, 0) gSLR mode has a strength that is much weaker than TE₀(0, ±1) since the energy coupled to TM₀ mode is weaker than that coupled to TE₀ (**Fig. 1g**). It should be pointed out here that TE_x(0, ±1) and TM_s(±1, 0) have perpendicular coupling directions since TE modes and TM modes of same polarization transfer orthogonally inside the slab (**Fig. 1g**). The coupling direction of TE_x(0, ±1) modes is parallel to the excitation polarization while that of TM_x(±1, 0) modes is orthogonal (**Fig. 1h** and **i**). The rectangular unit cell design makes it easy to differentiate

coupling direction by peak position. Under x-polarized excitation $TM_x(\pm 1, 0)$ modes are at longer wavelengths, while $TE_x(0, \pm 1)$ modes are at longer wavelength under y-polarized excitation (**Fig. S2**). A slight redshift is observed at strong peaks ($TE_0(0, \pm 1)$ and $TE_1(0, \pm 1)$) in **Fig. 1b** and **f**), which is caused by strong coupling strength^{18,23,46}. The strong coupling strength of $TE_0(0, \pm 1)$ mode also causes field distortion near AuNPs (**Fig. 1h**), which is an evidence for interactions of guided light and AuNPs. For weakly coupled $TM_0(\pm 1, 0)$ mode, the field distribution is much similar to that of GMR as the interaction is weak (**Fig. 1i**).

Strong resonances also occur near $TE_x(0, \pm 1)$ modes even corresponding TE modes are cut-off. This could be attributed to reflections at finite boundaries⁴¹. The similar field distribution to $TE_x(0, \pm 1)$ modes implies that these resonances are transition states of gSLR (**Fig. S3**). A clear transiting path from resonance in superstrate to gSLR can be found in both simulation and experiment (**Fig. 1a** and **c**, **Fig. S2**). However, with the guided modes being cut-off, TM and $TE_x(\pm 1, \pm 1)$ modes totally turn off when the slab is not thick enough. This is because when guided modes are cutoff, energy transferred in the orthogonal direction (y-direction under x-polarized excitation) is negligible compare to that in the parallel direction (x-direction).

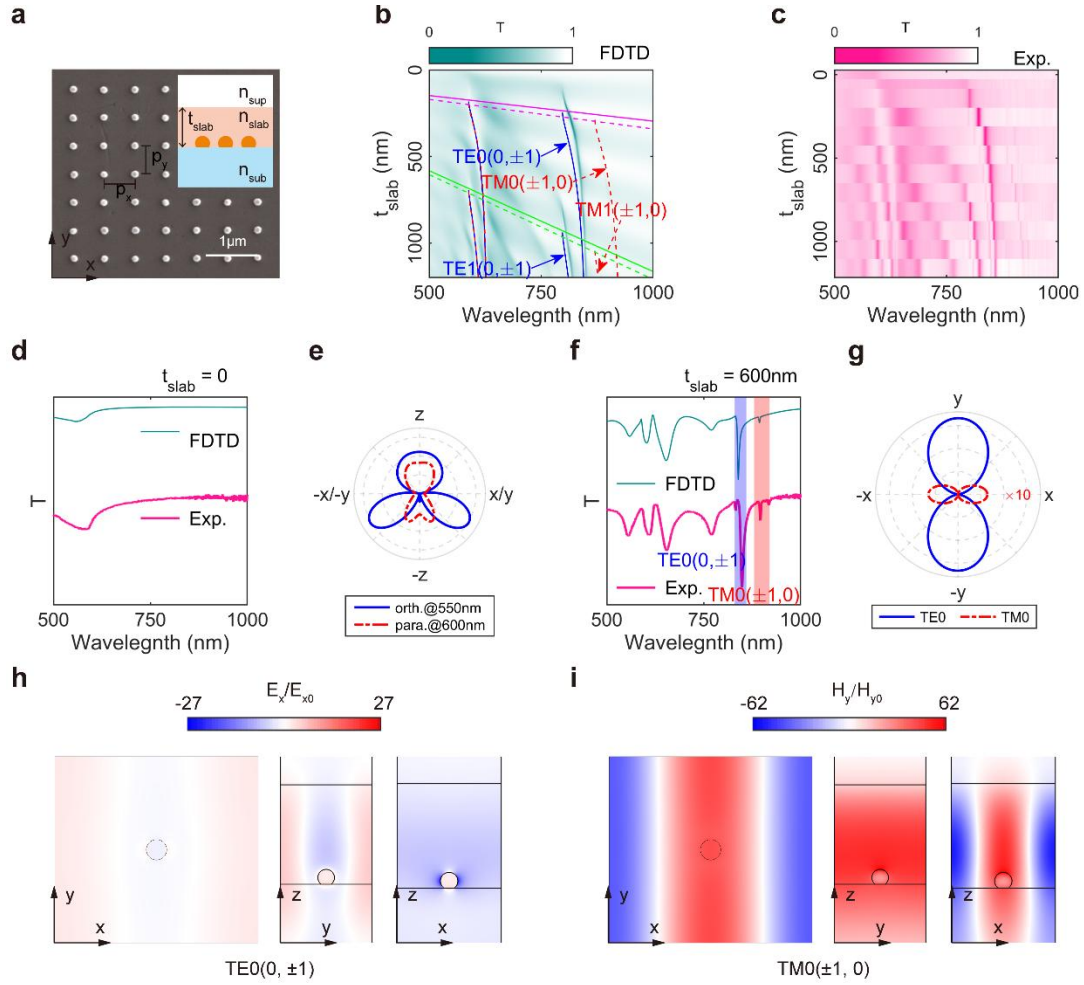


Fig. 1 Multimodal gSLR. (a) SEM image of the fabricated AuNPA metasurface. Each AuNP has a diameter of ~ 100 nm and a height of ~ 90 nm. Lattice constant in x (p_x) and y (p_y) directions are 600 nm and 550 nm. Insert shows the lateral view of gSLR configuration. The AuNPA are fabricated on quartz substrate and embedded in a finite polymer slab (photoresist). (b) Simulated gSLR mode evolution with the increase of slab thickness. $TE_x(0, \pm 1)$ and $TM_x(\pm 1, 0)$ gSLR modes are labeled by blue solid and red dash curves. Unlabeled curve at the left corresponds to $TE_x(\pm 1, \pm 1)$ and $TM_x(\pm 1, \pm 1)$ gSLR modes. Solid and dash straight lines indicate cut-off thickness of TE and TM waveguide modes, specifically, magenta for TE_0 (TM_0) and green for TE_1 (TM_1). (c) Experimental results of gSLR modes evolution. (d) Simulated and measured transmittance spectra of AuNPA on quartz substrate and in air superstrate, (e) Radiation pattern of a single AuNP on quartz in air, (f) Simulated and measured gSLR transmittance spectra of 600 nm slab. Light blue and light red shadows are $TE_0(0, \pm 1)$ and $TM_0(\pm 1, 0)$ gSLR mode positions. (g) Guided mode radiation pattern of single AuNP in 600 nm slab at $TE_0(0, \pm 1)$ and $TM_0(\pm 1, 0)$ gSLR mode positions in (f). (h) and (i) are field distribution of $TE_0(0, \pm 1)$ and $TM_0(\pm 1, 0)$ gSLR modes.

2.2 Tunable mode strength of gSLR

Dipole emission inside waveguides has been proved to be position-dependent⁵⁷. As the scattering of simple nanoparticles can be modeled as dipoles^{20,45}, a reasonable hypothesis is

that gSLR of a metasurface is positionally tunable. As is illustrated in **Fig. 2a**, by changing vertical position of the metasurface, the radiation pattern of individual nanoparticles changes. Consequently, corresponding gSLR modes coupling strength can be controlled. Numerical simulation shows that $TE1(0, \pm 1)$ mode undergoes an on-off-on change and $TM1(\pm 1, 0)$ mode goes off-on-off-on when the metasurface is elevated from the bottom to the top of a 1200 nm thick slab. Other gSLR modes also show strength changes during this lifting (**Fig. 2b**). Specifically, when the metasurface is vertically displaced by 500 nm, the $TE0(0, \pm 1)$ redshifts and shows a deeper dip, the originally weak $TM0(\pm 1, 0)$ mode is further suppressed, the strong $TE1(0, \pm 1)$ mode is totally turned off while the $TM1(\pm 1, 0)$ mode reaches its strongest strength. Experiment results support simulations very well (**Fig. 2c**). The same as previous discussion, peak splits are caused by oblique incidence. To explore the mechanism of the tunability, guided modes radiation patterns of single AuNP in waveguide at 0 and 500 nm vertical distances are extracted. After displacing, the far field intensity of $TE0$ mode gets stronger (**Fig. 2d**), bringing stronger gSLR coupling strength, causing a redshifted and strengthened dip. Meanwhile, an one order weakening in far field intensity of $TM0$ mode accounts for the suppression of $TM0(\pm 1, 0)$ gSLR mode (**Fig. 2e**). The reason for the fading of $TE1(0, \pm 1)$ gSLR mode lies here that the far field electric field strength that coupled to $TE1$ mode at ~ 820 nm when AuNPs are at the bottom of the slab is two orders of that when AuNPs are offset by 500 nm (**Fig. 2f**). At the same time, the far field electric field strength which coupled to $TM1$ mode at 875 nm when AuNPs seat on the substrate is only one tenth of that when lifted by 500 nm (**Fig. 2g**), explaining for the turning on of $TM0(\pm 1, 0)$ gSLR mode. In general, by engineering radiation patterns of nanoparticles in a metasurface, gSLR modes can be actively tuned on-demand.

When the metasurface touches the slab upper boundary, all gSLR modes are wearing off. This fading can be attributed to a transition from gSLR to GMR^{52,53}. When the metasurface totally moved outside the slab, gSLR is forbidden and GMR rises, as is illustrated in **Fig. 3a**. Compared to gSLR, GMR modes have much higher Q-factors (left panel in **Fig. 3b**). This is because light is shined into the waveguide by diffractions of the meta-grating and transfers inside the slab, which means the coupled light has little interaction with the lossy plasmonic meta-grating outside, avoiding losses caused by plasmonic materials in used. While in the

case of gSLR, coupled light is scattered by AuNPs and strongly interacts with optically lossy plasmonic nanoparticles, resulting in stronger damping and lower Q-factors. This conclusion is supported by the field distribution difference of GMR and gSLR modes. As is show in **Fig. 3c**, the enhanced electric field is main restrained in waveguide slab with minor distortion near AuNP for GMR TE₀ mode. While for gSLR TE₀(0, ±1) mode, though the guided characteristic is still obvious, the electric field enhancement near the particle is much larger than in other areas (**Fig. 3d**). The localized field enhancement roots in strong light-matter interactions with AuNPs. Moreover, given that energy proportion of high order diffractions takes a small part in total, the coupling efficiency of GMR under normal incidence is usually low. As a result, excitation and observation of GMRs need elaborate skills, for example, using cross polarized measurement to exclude uncoupled background noise⁵², because of which most of reported ultra-high-Q GMRs work in reflection mode^{52,53}. If without using those techniques, GMR modes will be flooded by background signal and turn undetectable. Nevertheless, the much higher coupling efficiency given by scattering make gSLRs easier to access. As in **Fig. 3b**, under the same experiment condition, gSLR modes are prominent while GMR modes are hard to recognize. This difference may privilege gSLR in applications that require high coupling efficiencies and moderately high Q-factors, for example, solar energy harvesting⁵⁸.

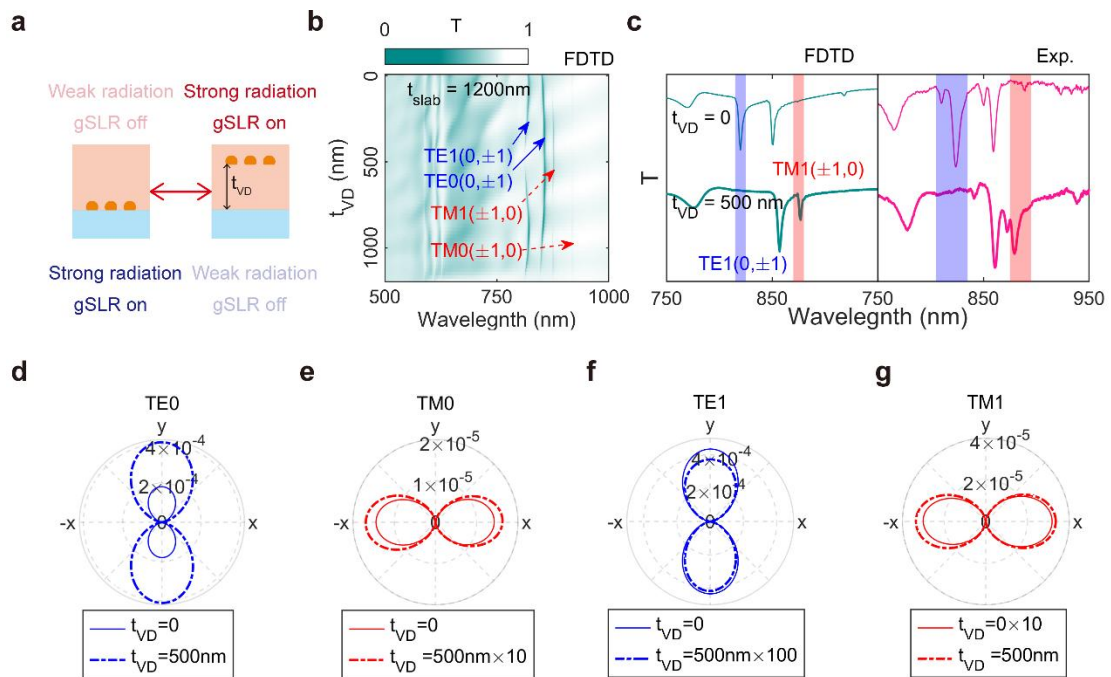


Fig. 2 Tunable mode strength of gSLR. (a) Schematics of positionally tuning gSLR. (b) Simulated tunable gSLR, (c) Simulated and experiment transmittance spectra of the metasurface with $t_{\text{slab}} = 1200$ nm, $t_{\text{VD}} = 0$ (top) and $t_{\text{VD}} = 500$ nm (bottom), (d-g) Guided TE₀, TM₀, TE₁ and TM₁ mode radiation pattern at $t_{\text{VD}} = 0$ and $t_{\text{VD}} = 500$ nm.

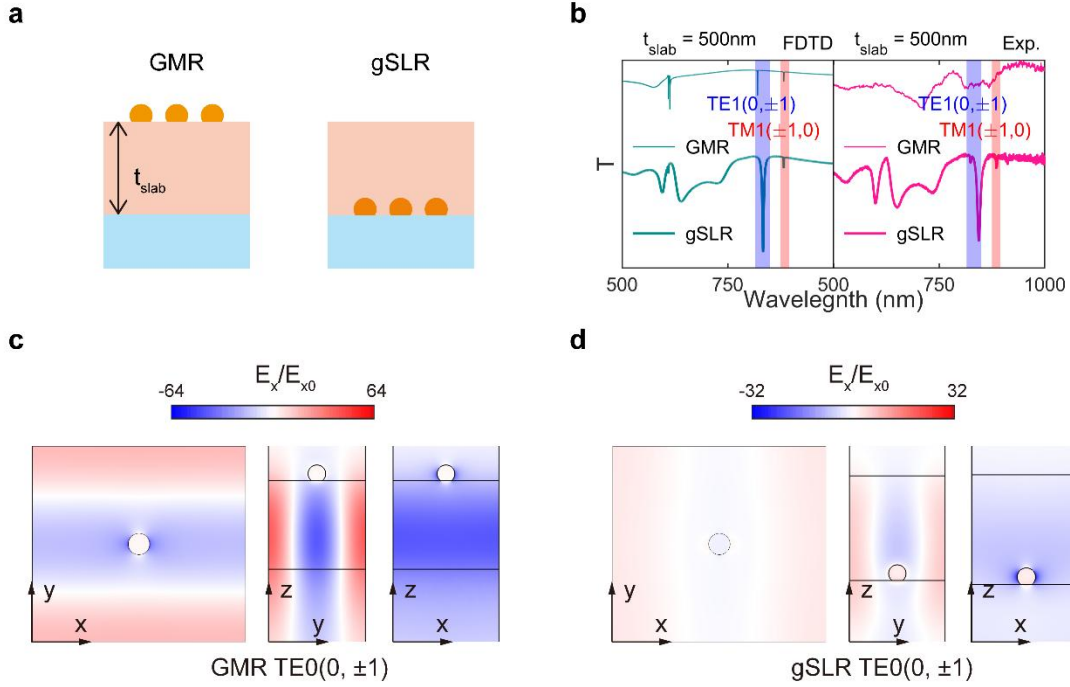


Fig. 3 Comparison between GMR and gSLR. (a) Schematics of GMR and gSLR configuration, (b) Simulated and experimental transmittance of GMR and gSLR, (c) field distribution of GMR TE₀(0, ±1) mode, (d) field distribution of gSLR TE₀(0, ±1) mode.

2.3 Polarization tuning of gSLR

As has been discussed above, gSLR supports multiple resonances in orthogonal coupling directions. Taking advantages of the rectangular lattice configuration, number of modes in one spectrum can be further enriched by altering the excitation polarization. As is shown in **Fig. 4**, TE₀(0, ±1) and TE₁(±1, 0) modes turn from their strongest to off state while peak intensities of TE₁(±1, 0) and TE₀(±1, 0) increases from zero to their highest, when the excitation polarization rotates from x-direction to y-direction. Attentions should be paid to this that peak positions never change though their intensities decrease or increase, unlike being tuned by vertical positions. This is because altering the excitation polarization only changes energy proportion allocated to gSLR modes that couples to x-direction and that to y-direction. The modal coupling strength or the density-of-state of each mode is defined by the configuration and independent from excitation strength in linear region.

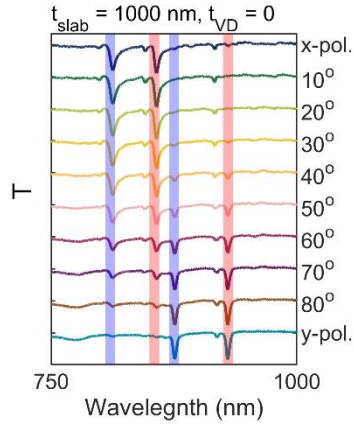


Fig. 4 Excitation polarization switching gSLR. The shadowed strips indicate TE1(0, ± 1), TE0(0, ± 1), TE1(± 1 , 0) and TE0(± 1 , 0) from left to right.

2.4 Discussions

Firstly, it should be emphasized here that the slab waveguide only modulates the radiation pattern of nanoparticles inside the slab instead of changing the optic response of them. Specifically, no MD is excited for a 100 nm gold nanosphere (AuNS) in a slab waveguide even TM gSLR modes are arisen from a 100 nm AuNS lattice. This conclusion can be proved by calculating the guided radiation pattern of an ED in a slab waveguide. **Figure S7** shows the tailored radiation pattern of an ED at positions the same as a 100 nm AuNS case in section 2.2. The calculated guided radiation patterns of the ED are similar to those of an AuNS under the same configuration (**Fig. 1g**).

Secondly, though discussions in this manuscript mainly focus on plasmonic dipole lattices, the conclusion and mythology can be applied to multipole and dielectric lattices such as silicon nanoparticles. **Figure S8a** shows simulated results of gSLR generated in a silicon nanosphere metasurface. Positional tunability also works for dielectric metasurfaces (**Fig. S8b**). The difference is that TM gSLR modes of dielectric metasurfaces are stronger compared to those of plasmonic metasurfaces with the same configuration, considering the intrinsic MDs in large dielectric nanoparticles.

Finally, the wavelength tuning range of gSLR is determined by the effective index range of the slab waveguide. In above discussion, the tuning range is limited by the small index contrast between the polymer slab ($n = 1.56$) and the quartz substrate ($n = 1.45$). A wider tuning range is attainable once substituting the slab with high index dielectrics or using metal substrate.

3 Conclusion

In summary, we proposed and experimentally demonstrated a multimodal gSLR by embedding the metasurface in a thin slab. Taking advantages of slab waveguide to conduct light in the metasurface plane, gSLR can occur in sharply contrasted superstrate and substrate environment once waveguide mode isn't cut-off, which largely relieves the index matching requirement for SLR generation. Meanwhile, multimodal resonances with desired resonant peak number, peak position and coupling direction can be rationally designed by adjusting array lattice constant, slab thickness or cladding index. Moreover, by modulating radiation pattern of consisting nanoparticles through vertical position in the slab, gSLR is equipped with a flexible tunability on mode strength. The asymmetric-environment-adaptive, easy-to-excite, multimodal and actively tunable traits of gSLR will promote potential applications in many fields like optoelectronics and biosensors.

Method

Simulations

Finite-difference time domain (FDTD) simulations were run to calculate scattering cross sections of individual nanoparticles and transmittance spectra of arrays. For arrays, the simulation was performed in a unit cell, using periodic boundary conditions in the in-plane dimensions and perfect matched layers at the out-of-plane dimension. A small negative imaginary part ($k = \sim 10^{-4}$) was added to environment to improve the convergency. The free-space and guided radiation pattern of individual nanoparticles were obtained by finite element method solver and an open-source algorithm⁵³.

Sample fabrication

The gold nanodisk array (AuNDA) samples were fabricated by a template method. Briefly, a silicon nanohole array mold was made by electron beam lithography (EBL) and reactive ion etching (RIE). Then a poly(diallyldimethylammonium chloride) (PDAC) film was deposited on the mold via spincoating of 0.5% aqueous PDAC solution. A nanohole array template was fabricated via depositing 2 nm/100 nm Cu/Ag on the PDAC capped silicon mold and transferred onto a quartz substrate with the help of water. The AuNDA was made by

depositing 1nm/50nm Cr/Au and etching the silver template. Finally, the fabricated sample was annealed at 1000 °C for 2h to improve uniformity⁵¹.

Optical measurement

The measurement set-up is depicted in Fig. S5. Transmittance spectra were obtained by a spectrometer under the illumination of a halogen lamp. A 10X objective with NA of 0.3 was used to collecting signal. An iris was placed at the back focal plane of the objective to ensure that only plane wave light that normal to the array was collected. The slab waveguide was made by spincoating diluted negative photoresist (SU8-2000.5, 5 times diluted in anisole) on the sample. The waveguide-thickness increasing was realized by a layer-by-layer coating-curing process.

References

- 1 Liao, J.-W. *et al.* Highly Localized Surface Plasmon Nanolasers via Strong Coupling. *Nano Letters* **23**, 4359–4366 (2023).
- 2 Fernandez-Bravo, A. *et al.* Ultralow-threshold, continuous-wave upconverting lasing from subwavelength plasmons. *Nature Materials* **18**, 1172–1176 (2019).
- 3 Dhama, R. *et al.* All-optical switching based on plasmon-induced Enhancement of Index of Refraction. *Nature Communications* **13**, 3114 (2022).
- 4 Wang, H. *et al.* All-optical ultrafast polarization switching with nonlinear plasmonic metasurfaces. *Science Advances* **10**, eadk3882 (2024).
- 5 Mejía-Salazar, J. R. & Oliveira, O. N. Plasmonic Biosensing. *Chemical Reviews* **118**, 10617-10625 (2018).
- 6 Ahmadvand, A. & Gerislioglu, B. Photonic and Plasmonic Metasensors. *Laser & Photonics Reviews* **16**, 2100328 (2021).
- 7 Li, G., Zhang, S. & Zentgraf, T. Nonlinear photonic metasurfaces. *Nature Reviews Materials* **2**, 17010 (2017).
- 8 Li, C. *et al.* Second Harmonic Generation from a Single Plasmonic Nanorod Strongly Coupled to a WSe₂ Monolayer. *Nano Letters* **21**, 1599-1605 (2020).
- 9 Overvig, A. & Alù, A. Diffractive Nonlocal Metasurfaces. *Laser & Photonics Reviews* **16**, 2100633 (2022).
- 10 Guan, J. *et al.* Far-field coupling between moiré photonic lattices. *Nature Nanotechnology* **18**, 514-520 (2023).
- 11 Azzam, S. I., Shalaev, V. M., Boltasseva, A. & Kildishev, A. V. Formation of Bound States in the Continuum in Hybrid Plasmonic-Photonic Systems. *Physical Review Letters* **121**, 253901 (2018).
- 12 Liang, Y. *et al.* Bound States in the Continuum in Anisotropic Plasmonic Metasurfaces. *Nano Letters* **20**, 6351-6356 (2020).
- 13 Kang, H. *et al.* Stabilization of Silver and Gold Nanoparticles: Preservation and Improvement of Plasmonic Functionalities. *Chemical Reviews* **119**, 664-699 (2018).
- 14 Wang, M. *et al.* Tunable Fano Resonance and Plasmon–Exciton Coupling in Single Au Nanotriangles on Monolayer WS₂ at Room Temperature. *Advanced Materials* **30**,

- 1705779 (2018).
- 15 Fang, J. *et al.* Tunable Couplings of Photons with Bright and Dark Excitons in Monolayer Semiconductors on Plasmonic-Nanosphere-on-Mirror Cavities. *The Journal of Physical Chemistry C* **127**, 9105-9112 (2023).
- 16 Ma, J., Wang, X., Feng, J., Huang, C. & Fan, Z. Individual Plasmonic Nanoprobes for Biosensing and Bioimaging: Recent Advances and Perspectives. *Small* **17**, 2004287 (2021).
- 17 Liu, Y. *et al.* Label-Free Ultrasensitive Detection of Abnormal Chiral Metabolites in Diabetes. *ACS Nano* **15**, 6448-6456 (2021).
- 18 Utyushev, A. D., Zakomirnyi, V. I. & Rasskazov, I. L. Collective lattice resonances: Plasmonics and beyond. *Reviews in Physics* **6**, 100051 (2021).
- 19 Wang, B. *et al.* High-Q Plasmonic Resonances: Fundamentals and Applications. *Advanced Optical Materials* **9**, 2001520 (2021).
- 20 Bin-Alam, M. S. *et al.* Ultra-high-Q resonances in plasmonic metasurfaces. *Nature Communications* **12**, 974 (2021).
- 21 Kravets, V. G., Kabashin, A. V., Barnes, W. L. & Grigorenko, A. N. Plasmonic Surface Lattice Resonances: A Review of Properties and Applications. *Chemical Reviews* **118**, 5912-5951 (2018).
- 22 Cherqui, C., Bourgeois, M. R., Wang, D. & Schatz, G. C. Plasmonic Surface Lattice Resonances: Theory and Computation. *Accounts of Chemical Research* **52**, 2548-2558 (2019).
- 23 Augu  , B. & Barnes, W. L. Collective Resonances in Gold Nanoparticle Arrays. *Physical Review Letters* **101** (2008). <https://doi.org/10.1103/PhysRevLett.101.143902>
- 24 Wang, W. *et al.* The rich photonic world of plasmonic nanoparticle arrays. *Materials Today* **21**, 303-314 (2018).
- 25 Augu  , B., Benda  a, X. M., Barnes, W. L. & Garc  a de Abajo, F. J. Diffractive arrays of gold nanoparticles near an interface: Critical role of the substrate. *Physical Review B* **82** (2010).
- 26 Mahi, N. *et al.* In Depth Investigation of Lattice Plasmon Modes in Substrate-Supported Gratings of Metal Monomers and Dimers. *The Journal of Physical Chemistry C* **121**, 2388-2401 (2017).
- 27 Kelavuori, J. *et al.* Thermal Control of Plasmonic Surface Lattice Resonances. *Nano Letters* **22**, 3879-3883 (2022).
- 28 Qi, X., P  rez, L. A., Alonso, M. I. & Mihi, A. High Q-Factor Plasmonic Surface Lattice Resonances in Colloidal Nanoparticle Arrays. *ACS Applied Materials & Interfaces* **16**, 1259-1267 (2024).
- 29 Andreas Tittl, A. L., Mingkai Liu, Filiz Yesilkoy, Duk-Yong Choi, Dragomir N. Neshev, Yuri S. Kivshar, Hatice Altug. Imaging-based molecular barcoding with pixelated dielectric metasurfaces. *Science* **360**, 1105-1109 (2018).
- 30 Danilov, A. *et al.* Ultra-narrow surface lattice resonances in plasmonic metamaterial arrays for biosensing applications. *Biosensors and Bioelectronics* **104**, 102-112 (2018).
- 31 Yang, H. *et al.* Detailed formation mechanism of sharp plasmonic lattice modes on Au hemi-ellipsoid arrays in inhomogeneous environment. *Journal of Physics D:*

- Applied Physics* **56** (2023-08-11).
- 32 Men, D. *et al.* Surface lattice resonance in an asymmetric air environment of 2D Au near-spherical nanoparticle arrays: impact of nanoparticle size and its sensitivity. *Journal of Materials Chemistry C* **12**, 3254 (2024).
- 33 Li, L. & Wu, W. Bimodal surface lattice resonance sensing based on asymmetric metasurfaces. *Applied Physics Letters* **124**, 071701 (2024).
- 34 Li, Y. *et al.* Ultra-narrow band perfect absorbance induced by magnetic lattice resonances in dielectric dimer metamaterials. *Results in Physics* **39**, 105730 (2022).
- 35 Yu, A., Li, W., Wang, Y. & Li, T. Surface lattice resonances based on parallel coupling in metal-insulator-metal stacks. *Optics Express* **26**, 20695 (2018).
- 36 Guan, J. *et al.* Plasmonic Nanoparticle Lattice Devices for White-Light Lasing. *Advanced Materials* **35**, 2103262 (2021).
- 37 Wang, D. *et al.* Band-edge engineering for controlled multi-modal nanolasing in plasmonic superlattices. *Nature Nanotechnology* **12**, 889-894 (2017).
- 38 Baur, S., Sanders, S. & Manjavacas, A. Hybridization of Lattice Resonances. *ACS Nano* **12**, 1618-1629 (2018).
- 39 Braïk, M. *et al.* Hybridization of surface lattice modes: towards plasmonic metasurfaces with high flexible tunability. *Nanophotonics* **12**, 2179–2188 (2023).
- 40 Lim, T.-L. *et al.* Fourier-Engineered Plasmonic Lattice Resonances. *ACS Nano* **16**, 5696–5703 (2022).
- 41 Reshef, O. *et al.* Multiresonant High-Q Plasmonic Metasurfaces. *Nano Letters* **19**, 6429-6434 (2019).
- 42 Volk, K., Fitzgerald, J. P. S. & Karg, M. In-Plane Surface Lattice and Higher Order Resonances in Self-Assembled Plasmonic Monolayers: From Substrate-Supported to Free-Standing Thin Films. *ACS Applied Materials & Interfaces* **11**, 16096-16106 (2019).
- 43 Boddeti, A. K. *et al.* Long-Range Dipole–Dipole Interactions in a Plasmonic Lattice. *Nano Letters* **22**, 22-28 (2021).
- 44 Huttunen, M. J., Dolgaleva, K., Törmä, P. & Boyd, R. W. Ultra-strong polarization dependence of surface lattice resonances with out-of-plane plasmon oscillations. *Optics Express* **24**, 28279 (2016).
- 45 Novotny, L. & van Hulst, N. Antennas for light. *Nature Photonics* **5**, 83-90 (2011).
- 46 Zakomirnyi, V. I. *et al.* Collective lattice resonances in arrays of dielectric nanoparticles: a matter of size. *Optics Letters* **44**, 5743-5746 (2019).
- 47 Li, J., Verellen, N. & Van Dorpe, P. Engineering electric and magnetic dipole coupling in arrays of dielectric nanoparticles. *Journal of Applied Physics* **123**, 083101 (2018).
- 48 Lin, L. & Yi, Y. Orthogonal and parallel lattice plasmon resonance in core-shell SiO₂/Au nanocylinder arrays. *Optics Express* **23**, 224136 (2015).
- 49 Vitrey, A., Aigouy, L., Prieto, P., García-Martín, J. M. & González, M. U. Parallel Collective Resonances in Arrays of Gold Nanorods. *Nano Letters* **14**, 2079-2085 (2014).
- 50 Muravitskaya, A., Movsesyan, A., Kostcheev, S. & Adam, P.-M. Polarization switching between parallel and orthogonal collective resonances in arrays of metal

- nanoparticles. *Journal of the Optical Society of America B* **36**, 65-70 (2019).
- 51 Deng, S. *et al.* Ultranarrow plasmon resonances from annealed nanoparticle lattices. *Proc Natl Acad Sci U S A* **117**, 23380-23384 (2020).
- 52 Huang, L. *et al.* Ultrahigh-Q guided mode resonances in an All-dielectric metasurface. *Nature Communications* **14**, 3433 (2023).
- 53 Quaranta, G., Basset, G., Martin, O. J. F. & Gallinet, B. Recent Advances in Resonant Waveguide Gratings. *Laser & Photonics Reviews* **12**, 1800017 (2018).
- 54 Gutha, R. R., Sadeghi, S. M., Sharp, C., Hatef, A. & Lin, Y. Multi-order surface lattice resonances and dark mode activation in metallic nanoantenna arrays. *Journal of Applied Physics* **125**, 023103 (2019).
- 55 Le-Van, Q. *et al.* Enhanced Quality Factors of Surface Lattice Resonances in Plasmonic Arrays of Nanoparticles. *Advanced Optical Materials* **7**, 1801451 (2019).
- 56 Yang, F. *et al.* Fabrication of Centimeter-Scale Plasmonic Nanoparticle Arrays with Ultranarrow Surface Lattice Resonances. *ACS Nano* **17**, 725-734 (2022).
- 57 Ramezani, M., Lozano, G., Verschuuren, M. A. & Gómez-Rivas, J. Modified emission of extended light emitting layers by selective coupling to collective lattice resonances. *Physical Review B* **94**, 125406 (2016).
- 58 Zhukovsky, S. V. *et al.* Enhanced Electron Photoemission by Collective Lattice Resonances in Plasmonic Nanoparticle-Array Photodetectors and Solar Cells. *Plasmonics* **9**, 283–289 (2014).

Supporting Information

Waveguide Tailored Radiation Pattern of Nanoparticles for Tunable Multimodal Guided Surface Lattice Resonances in Asymmetric Environment

Suichu Huang¹, Kan Yao², Wentao Huang¹, Xuezheng Zhao^{1, *}, Yuebing Zheng^{2, *}, Yunlu Pan^{1, *}

1 Key Laboratory of Micro-Systems and Micro-Structures Manufacturing of Ministry of Education and School of Mechatronics Engineering, Harbin Institute of Technology, Harbin 150001, China

2 Walker Department of Mechanical Engineering, Material Science and Engineering Program and Texas Material Institute, The University of Texas at Austin, Austin TX 78712, United States

*Corresponding author. Email: zhaoxz@hit.edu.cn, zheng@austin.utexas.edu, yunlupan@hit.edu.cn

Section 1 Waveguided modes in a three-layer slab waveguide and gSLR

When $n_2 > n_3 > n_1$, a three-layer structure forms a slab waveguide. We firstly consider the transverse electric (TE, E//y) case. For the guided modes, the field intensity goes to zero at the infinity. So the electric field can be expressed as

$$E_y(z) = A \exp(-\beta_1 z), z > \frac{t}{2} \quad (1-1.a)$$

$$E_y(z) = B \cos(\beta_2 z + \varphi), -\frac{t}{2} \leq z \leq \frac{t}{2} \quad (1-1.b)$$

$$E_y(z) = C \exp(\beta_3 z), z < -\frac{t}{2}, \quad (1-1.c)$$

where, $\beta_1 = \sqrt{k^2 - n_1^2 k_0^2}$, $\beta_2 = \sqrt{n_2^2 k_0^2 - k^2}$, $\beta_3 = \sqrt{k^2 - n_3^2 k_0^2}$, and $k = \sqrt{k_x^2 + k_y^2}$ is the in-planal wave vector component.

Given

$$H_x = -\frac{i}{\omega \mu_0} \frac{\partial E_y}{\partial z}, \quad (1-2)$$

The magnetic field can be derived as

$$H_x(z) = \frac{i}{\omega \mu_0} \beta_1 A \exp(-\beta_1 z), z > \frac{t}{2} \quad (1-3.a)$$

$$H_x(z) = \frac{i}{\omega \mu_0} \beta_2 B \sin(\beta_2 z + \varphi), -\frac{t}{2} \leq z \leq \frac{t}{2} \quad (1-3.b)$$

$$H_x(z) = -\frac{i}{\omega \mu_0} \beta_3 C \exp(\beta_3 z), z < -\frac{t}{2}. \quad (1-3.c)$$

Since E_y and H_x are continuous at the interfaces, we have

$$A \exp\left(-\beta_1 \frac{t}{2}\right) = B \cos\left(\beta_2 \frac{t}{2} + \varphi\right) \quad (1-4.a)$$

$$D \exp\left(-\beta_3 \frac{t}{2}\right) = B \cos\left(-\beta_2 \frac{t}{2} + \varphi\right) \quad (1-4.b)$$

$$\beta_1 A \exp\left(-\beta_1 \frac{t}{2}\right) = \beta_2 B \sin\left(\beta_2 \frac{t}{2} + \varphi\right) \quad (1-4.c)$$

$$-\beta_3 A \exp\left(-\beta_1 \frac{t}{2}\right) = \beta_2 B \sin\left(-\beta_2 \frac{t}{2} + \varphi\right) \quad (1-4.d)$$

$$\beta_1 \cdot (2 - 4.a) - (2 - 4.c): \quad \tan\left(\beta_2 \frac{t}{2} + \varphi\right) = \frac{\beta_1}{\beta_2} \quad (1-5.a)$$

$$\beta_3 \cdot (2 - 4.b) + (2 - 4.d): \quad \tan\left(-\beta_2 \frac{t}{2} + \varphi\right) = -\frac{\beta_3}{\beta_2} \quad (1-5.b)$$

By eliminating φ , the dispersion relationship of TE modes is

$$\tan(\beta_2 t) = \frac{\beta_2(\beta_1 + \beta_3)}{\beta_2^2 - \beta_1 \beta_3}. \quad (1-6)$$

Similarly, the dispersion relationship of TM modes is

$$\tan(\beta_2 t) = \frac{\beta_2(c_{21}\beta_1 + c_{23}\beta_3)}{\beta_2^2 - c_{21}\beta_1 c_{23}\beta_3}, \quad (1-7)$$

where, $c_{21} = \frac{n_2^2}{n_1^2}$, $c_{23} = \frac{n_2^2}{n_3^2}$.

The effective index ($n_{\text{eff}} = k/k_0$) of each mode can be obtain by solving (1-6) and (1-7). For a given configuration, the cut-off wavelength is

$$\lambda_c = \frac{2\pi t \sqrt{n_2^2 - n_3^2}}{\left[\arctan\left(c_{21} \sqrt{\frac{n_2^2 - n_1^2}{n_2^2 - n_3^2}}\right) + j\pi \right]}, j = 0, 1, 2, \dots \quad (1-8)$$

Where, for TE modes, $c_{21} = 1$, for TM modes, $c_{21} = \frac{n_2^2}{n_1^2}$.

And for give wavelength, the cut-off thickness of the slab is

$$t_c = \frac{\lambda}{2\pi \sqrt{n_2^2 - n_3^2}} \left[\arctan\left(c_{21} \sqrt{\frac{n_2^2 - n_1^2}{n_2^2 - n_3^2}}\right) + j\pi \right], j = 0, 1, 2, \dots \quad (1-9)$$

The out-side in-coming light would not couple to these waveguided modes. However, should there be small structures inside the waveguide, some of the scattered light can match wave vectors of guided modes and thus transmits planarly inside the waveguide core layer. If the structure is an array, the travelling scattered light from nearby units will couple to each other, once their in-plane wave vectors satisfy

$$k_x = \frac{2\pi m}{P_x} \quad (1-10.a)$$

$$k_y = \frac{2\pi n}{P_y} \quad (1-10.b)$$

where $m = 0, 1, 2, \dots$, $n = 0, 1, 2, \dots$ and $m^2 + n^2 \neq 0$.

The origin of this kind of in-plane coupling is the same as surface lattice resonance (SLR), in which we define it as guided surface lattice resonance (gSLR). Substituting (1-10) into (1-6, 1-7), possible gLSR peaks positions can be determined. Taking advantages of rich modes of waveguides, gSLR possesses a multimodal nature. Figure S1 plots the mode evolution with slab thickness of a rectangular metasurface with lattice constants of 600 nm and 550 nm in x- and y-direction and under x-polarized normal incidence.

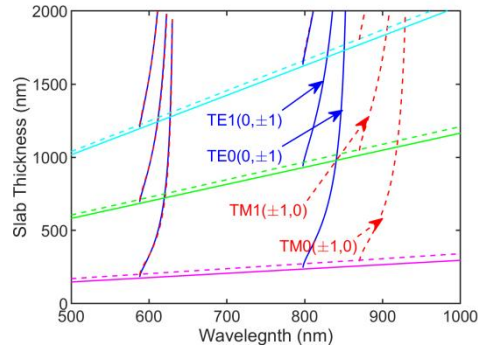


Fig. S1 Guided-SLR modes of a rectangular metasurface. Indices of the three-layer structure are 1, 1.56 and 1.45, respectively. Lattice constants are 600 nm and 550 nm in x- and y-direction, and the excitation is x-polarized. Solid and dash lines indicate cut-off thickness with solid lines for TE modes, dash lines for TM modes. From bottom to top, lines represent TE0, TM0, TE1, TM1, TE2 and TM2.

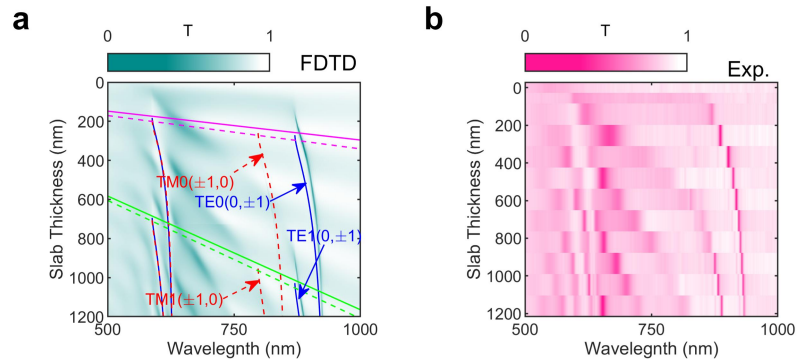


Fig. S2 Mode evolution of gSLR under y-polarized excitation in Air superstrate.

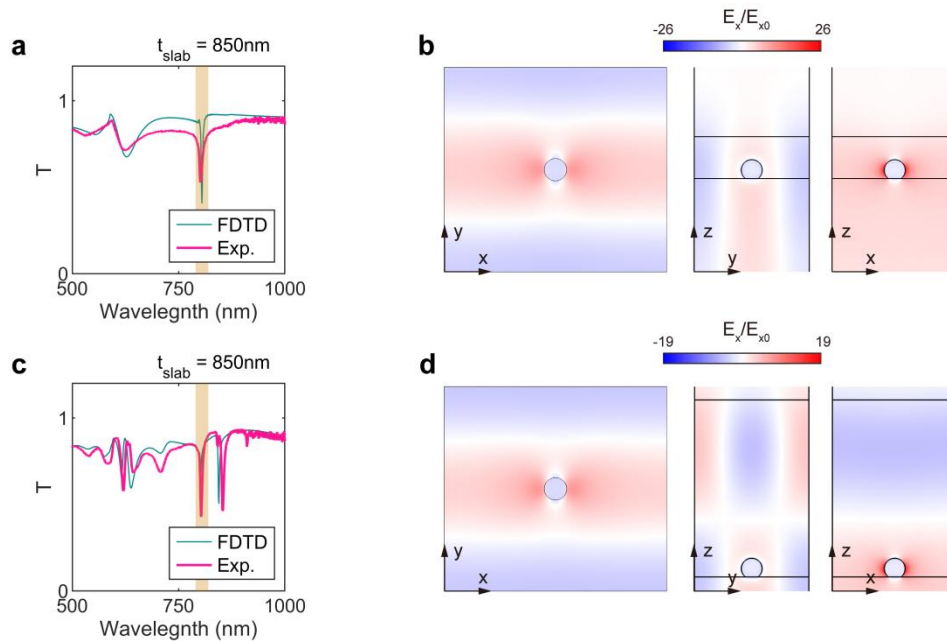


Fig. S3 Transitional resonances generated by reflections at slab boundaries. (a) Simulated and

experimental transmittance spectra of AuNPA metasurface in a 200 nm slab, the transitional resonance peak at ~ 802 nm is shadowed by orange, (b) Electric field distribution of resonances in (a), (c) Simulated and experimental transmittance spectra of AuNPA metasurface in a 850 nm slab, the transitional resonance peak at ~ 800 nm is shadowed by orange, (d) Electric field distribution of resonances in (c).

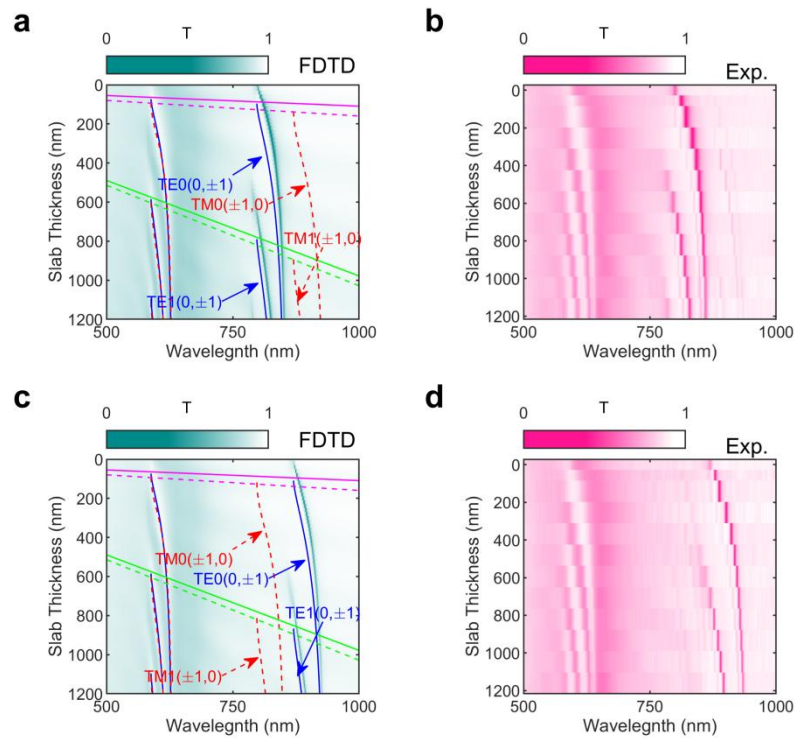


Fig. S4 Guided-SLR in EG superstrate. (a) Simulated transmittance spectra mapping in EG superstrate under x-polarized excitation, gLSR modes are labeled, (b) Experiment transmittance spectra mapping in EG superstrate under x-polarized excitation, (c) Simulated transmittance spectra mapping in EG superstrate under y-polarized excitation, gLSR modes are labeled, (d) Experiment transmittance spectra mapping in EG superstrate under y-polarized excitation.

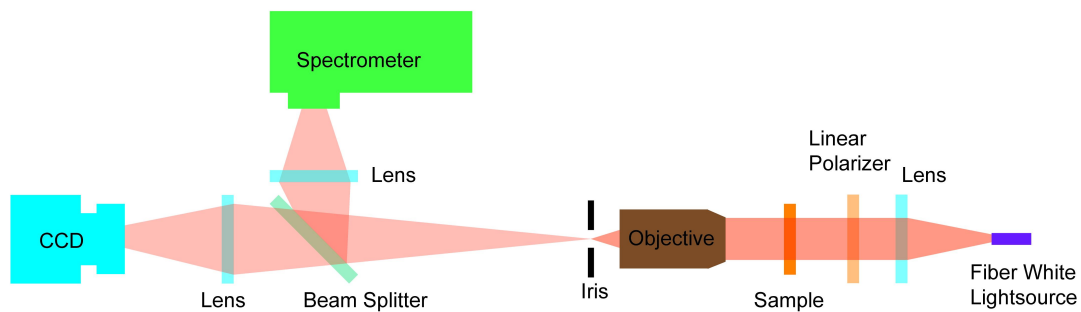


Fig. S5 Experimental set-up.

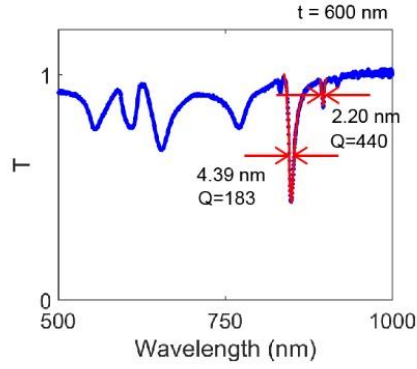


Fig. S6 Fano fitting and Q-factors of g-SLR.

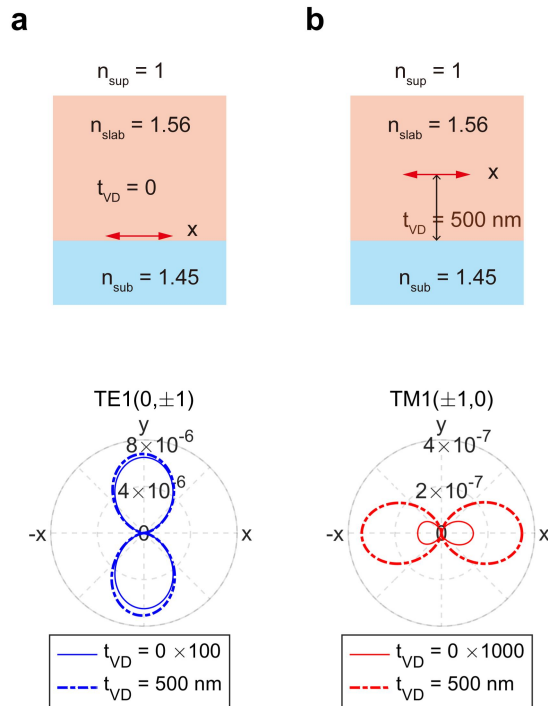


Fig. S7 Slab waveguide modulated radiative pattern of an electric dipole. Radiation pattern of an electric dipole near the boundary of the slab (a) and vertically displaced by 500 nm (b).

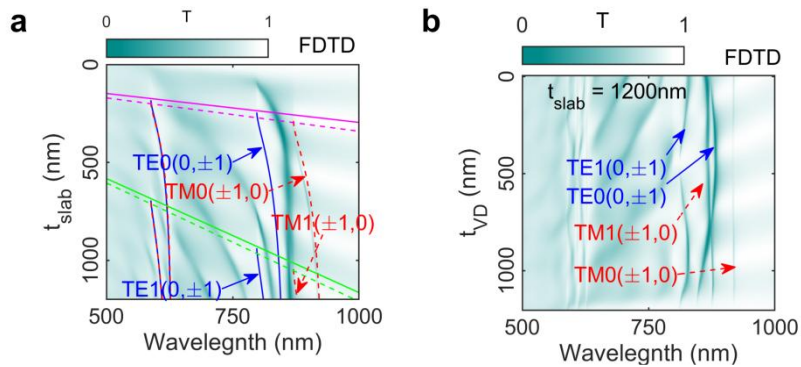


Fig. S8 Guided-SLR mode evolution of a silicon nanoparticle array metasurface. The metasurface consists of silicon nanospheres with a diameter of 130 nm. The lattice

configuration is the same as AuNPA metasurface. (a) gSLR mode evolution with the increase of slab thickness. (b) gSLR mode tunability by metasurface vertical position in slab.